Applied Surface Science 695 (2025) 162836

Contents lists available at ScienceDirect

Applied Surface Science

journal homepage: www.elsevier.com/locate/apsusc

Full length article

Probing additives for green lubricants with the aid of machine learning molecular dynamics: The case of gallate molecules for aqueous solutions

Huong Thi Thuy Ta [a], Mauro Ferrario [b], Sophie Loehlé [c], Maria Clelia Righi [a,*]

[a] Department of Physics and Astronomy, University of Bologna, 40127 Bologna, Italy
[b] Dipartimento di Scienze Fisiche, Informatiche e Matematiche, Università di Modena e Reggio Emilia, Via Campi 213/A, 41125 Modena, Italy
[c] TotalEnergies, OneTech Fuels& Lubricants, Research Center Solaize, 69360 Solaize, France

ARTICLE INFO

Keywords:
Green lubricants
Machine learning interaction potential
Tribochemical reactions
Gallates

ABSTRACT

To address the negative impacts of mineral oil-based lubricants on the environment and human health, eco-friendly lubricants based on aqueous solutions are increasingly being explored as an alternative for several tribological applications. The friction reduction properties of these lubricants crucially depends on the additives included in liquid of lower viscosity than oil. Great efforts are presently devoted to the search of molecular compounds able to function in boundary lubrication conditions, where the extreme pressures and low speeds make the liquid film become so thin that a direct contact between metal asperities can take place. Atomistic simulations represent a powerful tool to design lubricant additives as they can open a window on the sliding buried interface and unravel the mechanisms of function of candidate molecular compounds. However, while classical molecular dynamics simulations relying on empirical or reactive force fields poorly describe tribochemical reactions, the expensive cost of ab initio methods poses a big challenge when it comes to the required large system sizes and long time scales. In this study, we show how a machine-learning interaction potential derived from ab initio data can successfully be used to design lubricant additives. Considering the case of gallates at iron interfaces, our simulations highlight two key molecular features necessary for maintaining interfacial lubricity in boundary conditions: a strong anchoring of the molecules to the substrate, a function that for gallates is smartly activated by tribochemical reactions, and the presence of inert hydrocarbon tails that form a cushion that, thanks to Pauli repulsion, chemically isolates the covered substrate from any reactive counter-surface. These findings, of general validity, provides useful insights for designing new, environmental-friendly lubricants.

1. Introduction

Despite strict control on the life cycle of traditional mineral oil-based lubricants used in industrial applications and in the automotive universe, some degree of contamination remains unavoidable. Moreover, for several devices, like those with an open cutting system, the lubricating oil is forcefully emitted into the environment during operations, with a severe impact on the environment and human health. Thus, the search for effective yet sustainable and eco-friendly lubricants [1] has witnessed growing interests and "green lubricants" are being widely proposed, investigated and developed as the future generation of lubricants [2]. Traditional lubricants are derived mostly from petroleum. A mandatory but only partial route to safeguarding the environment lies in the application of best-practice recyclings, taking advantage of re-refined base oils lower carbon footprints, that permit a ~ 70% reduction in CO_2 emission and a similar reduction in production energy with respect to virgin base oils.

"Green" lubricants must be originated from renewable resources, biodegradable and eco-friendly, while maintaining the inherent essential properties of reducing friction, wear, corrosion, and oxidation. Aqueous-based lubricants are gaining increasing attention as sustainable alternatives to traditional mineral oil-based lubricants, thanks to their lower toxicity and environmental impact. However, to ensure effective performance under boundary lubrication conditions, where direct contact between surfaces is more likely, the use of additives is essential. These additives play a crucial role in enhancing the tribological properties, of aqueous lubricants, helping to reduce friction and wear. They can form protective films on surfaces, preventing nano asperity adhesion, thereby ensuring optimal performance even under high load and low-speed conditions. The selection and optimization of these additives are therefore essential for maximizing the effectiveness of aqueous lubricants in industrial and mechanical applications. In this work we explore the mechanism of function of gallates as

* Corresponding author.
E-mail address: clelia.righi@unibo.it (M.C. Righi).

https://doi.org/10.1016/j.apsusc.2025.162836
Received 18 January 2025; Received in revised form 21 February 2025; Accepted 27 February 2025
Available online 10 March 2025

friction reduction additives for aqueous-based lubricants. Gallic acid and its derivatives are being already widely used in pharmaceutical industry, [3,4] cosmetic, [5] and food industry [6] for their natural anti-oxidation function [7,8].. More recently, gallate molecules, introduced as an anti-oxidant agent in lubricant additives thanks to their capability to neutralize free radicals, showed promising results in reducing friction and wear [9–11]. However, in order to spread the application of gallates as lubricant additives, further investigation is needed to advance our understanding of the reduction mechanisms which are responsible for lubricity and the role played by the long alkyl chains that differentiate the gallate molecules between them and from gallic acid.

Computer simulations have played a crucial role in advancing the understanding of friction and wear reduction mechanisms in many tribochemical systems [12,13]. For example, atomistic scale simulations by *ab initio* molecular dynamics (AIMD) have been successfully used to provide insights into local chemical events, particularly on the formation and breaking of chemical bonds under harsh conditions in a variety of tribochemical systems such as metals, [14] oxides, [15–18] diamond, [19–21] silicates, [20,21] etc. At this scale, the sizes of the systems are limited to hundreds of atoms while the simulation time is within a scale of picoseconds. For lubricant additives such as fatty acids that have similar molecular structures as gallates, [22,23] it has been shown that these molecules tend to form a self-assembled monolayer (SAM) on a substrate thanks to the attraction between the head groups to the substrate [24]. The corresponding molecular dynamics (MD) simulation systems are commonly modeled as SAMs confined between substrates and described by empirical or reactive force fields (FF) [24–28]. These atomistic simulation results have provided useful information on the frictional dynamics of the systems, taking advantages of large simulation scales with modest computational costs. However, a satisfactory interpretation of atomic mechanisms of friction and wear is challenged by the poor description of chemical events and the lack of electron transfer information, leaving a big concern regarding the understanding of tribochemical reactions and tribofilm formation.

Recent development of machine learning applied to material modeling have opened a new era for atomistic simulations not only in tribology but also in other fields of physics, chemistry, biology, and materials. Machine learning interaction potentials (MLIP) inherited the accuracy of the *ab initio* description while maintaining the same efficiency as classical MD. The advantages of their adoption allow scientists to perform advanced studies with both long simulation time and large system sizes, of particular importance in the modeling of complex systems such as surfaces, interfaces, [29–34] or tribological systems [35–37]. In the present work a MLIP has been developed for a tribochemical system consisting of a group of gallate molecules acting as additives to form a lubricious tribofilm interacting between iron substrates. The MLIP was trained on a dataset constructed by means of density functional theory (DFT) and AIMD simulations in a sufficiently wide range of conditions to make sure that the whole potential energy surface of interest is well sampled. To this end an active learning method was applied to ensure possible physical and chemical alterations initiated under the tribological conditions in the systems are encompassed in the training process. The obtained MLIP enables us to perform large scale MD simulations with big models containing up to 10000 atoms in the nanosecond time scale of interest to investigate frictional properties. The obtained results permit to meaningfully evaluate the performance of these lubricant additives, rationalize the effect of alkyl chain lengths on the frictional properties, and progress further in the atomistic simulations of tribochemical processes.

In Section 2 we describe the computational setup of our calculations, in Section 3 we present the results from the computational modeling which are further discussed in Section 4.

2. Computational details

2.1. Density functional theory calculations

All *ab initio* calculations and AIMD simulations were performed using spin-polarized density functional theory (DFT) implemented in VASP package version 6.3.2 [38]. The projector-augmented wave (PAW) method was used for the interaction between electrons and ions. The exchange and correlation functional was described by the general gradient approximation (GGA) with the Perdew–Burke–Ernzerhof (PBE) [39]. The convergence threshold was set at 10^{-5} eV for the electronic energy and 10^{-2} eV/Å for the forces. Brillouin zone was sampled at the gamma point and the plane-wave expansion of the electronic wave function was truncated by setting the cutoff energy to 450 eV. The van der Waals (vdW) dispersion interactions between aromatic molecules were described by the DFT-D2 method of Grimme [40,41].

We considered as lubricant additives a group of four gallate molecules obtained from the gallic acid ($C_7H_6O_5$) by substituting an H atom by an alkyl chain. We considered propyl gallate (PG) butyl gallate (BG) octyl gallate (OG) and lauryl gallate (LG) with corresponding alkyl chains of C_3H_7, C_4H_9, C_8H_{17} and $C_{12}H_{25}$, respectively. The molecules were fully optimized before adding them on an Fe (110) surface within a supercell of area (14.20 × 12.05 Å) [2] with a thickness of four atomic layers. It is worth mentioning that the iron surface is anticipated to be exposed following the removal of surface oxide layers from metal-to-metal contact at asperities [42,43]. The pristine surface is chemically active, directly reacting with additive molecules. Consequently, the iron surface was selected as the adsorption substrate to represent the more severe contact conditions. The (110) surface of iron was chosen because it is the most stable surface of iron [44]. During geometrical optimization, the bottom layer of the iron substrate was kept frozen to better represent the effect of a bulk substrate. A vacuum layer of at least 13 Å was added on top of the molecular layer (or of the upper iron counter surface in interfacial systems) to effectively separate the systems of interest from its replicas along the z–direction, thus reducing unwanted effect due to the periodic boundary conditions. The adsorption energy per molecule $\left(E_{ads/mol}\right)$ was calculated by Eq. (1):

$$\left(E_{ads/mol}\right) = \frac{1}{n}\left(E_{total} - \left(E_{surf} + n \times E_{mol}\right)\right) \quad (1)$$

where E_{total} is the total energy of the surface interacting with the adsorbed molecules, E_{surf} and E_{mol} are the energies of the isolated surface and the isolated molecule, respectively, n is the number of gallate molecules adsorbed on the surface.

2.2. Data generation, MLIP training and validation

The initial training of the MLIP was started with the data generated from trajectories of AIMD and ReaxFF MD simulations. Relatively short, few picoseconds, AIMD simulations were performed for four kinds of systems: the bulk Fe, the Fe (110) surface, the bulk molecular liquids, and a system with 6 gallate molecules adsorbed on the Fe(110) surface (Fe-6GL). The reference geometries are presented in Figure S1a–d of the Supplementary Material, taking the case of BG as example. The systems were equilibrated at various temperature from 300 K to 3000 K to differentiate as much as possible the sampling of the configurations used to populate the initial dataset for the training. To integrate tribological effects, MD simulations under sliding conditions were performed for the models of Figure S1e using Lammps [45] with the ReaxFF force field [46]. The simulations were performed under a 1 GPa load at a temperature of 300 K for 100 ps, sampling atomic configurations every 1 ps for the calculations of energies and forces by DFT.

The DeepMD-kit package [47], written using Python/C++ languages and interfaced with TensorFlow [48], was used to perform the neural network training based on evaluation of atomic energies and forces. In particular, the DeepPot- SE (Deep Potential-Smooth Edition)

model [49] was used and to effectively improve the training dataset, additional data was generated through an active learning approach as proposed by Zhang et al.[50] The training model includes two networks, the embedding network and the fitting network, see Fig. 1 of Zhang et al. [49] The size of the embedding network was set to (25, 50, 100), and the size of the fitting network was set to (240, 240, 240). The cutoff radius was fixed to 6.0 Å and the descriptors decayed smoothly from 0.5 Å to 7.0 Å. The initial learning rate was set to 0.001 at the beginning of the training process to achieve a final value of 1×10^{-8}. The total numbers of training batches were 1×10^{6} for the training with the initial dataset and the iterations in the active learning process and 1.5×10^{6} for the final production training of the MLIP model. At the end of the training process, the MLIP was validated against the *ab initio* data using the validation set, which contained configurations not included in the training data.

Three independent MLIP were first trained separately for BG, OG, and LG. PG and BG molecules have very similar sizes, and indeed the potential initially trained for BG also worked fine for the shorter chain PG. The training and active learning processes are similar to that in our previous work for BG [35]. After several iterations, the exact number depending on the system, these potentials were able to properly describe the dynamics of the systems under sliding conditions. At this point, all the configurations were combined in a unique dataset, separating the training data from the validation data, and the active learning process was restarted, similarly to the procedure for separate molecules, but with the inclusion of systems with PG molecules. The active learning procedure was iterated for 5 generations, until a unique MLIP was obtained to describe all gallate molecules interaction with the Fe(110) surface. Further details about the training process and the active learning approach followed to optimize the training datasets for the applications in tribological conditions are presented in our previous publication [35].

2.3. Molecular dynamics simulations with machine learning interaction potentials

In tribological conditions the superficial oxides present on steel based surface are likely to be removed with molecules easily coming into direct contact with a pure iron surface, which significantly favor molecule chemisorption [23,35] with respect to iron hydroxides/oxides and it is expected that additives will play a beneficial role by alleviating direct Fe–Fe contacts. Therefore, simulations are focused on iron substrates sliding in the presence of the gallate molecules, in particular to investigate the specific role of the alkyl chain length. The Fe surface was selected as representative of the contact between two asperities in boundary lubrication regime. Large-scale molecular dynamics simulations were performed under sliding conditions using the final version of the MLIP by Lammps [45] version integrated within DeepMD-kit.

The simulation model is depicted in Fig. 1, containing one layer of gallate molecules confined between two iron surfaces. Two separate Nosé–Hoover thermostats, one for each of group of three inner layers of the upper and of the lower iron slabs, were applied to maintain a substrate temperature of 300 K. The unaltered Newton equations of motion were employed to integrate the dynamics of the atoms within the gallate layer, which is, therefore, only indirectly thermostatted through the interactions with the substrate. The tribological simulations were performed under five different loads ranging from 0.5 GPa to 2.5 GPa. Pressure was applied as external downward forces acting individually on the topmost atoms of the upper iron slab, while position constraining forces on the bottom-most atoms of the lower iron slab. The sliding was imposed by constraining the relative velocity (v = 50 m/s) along the x-direction between the uppermost and the bottom-most layer of iron atoms, i.e. the same atoms used to apply the external load. Periodic boundary conditions were applied along the x and y directions while in the z direction a vacuum layer of at least 30 Å was added to the top of the model. This was sufficient to prevent the emergence of unphysical configurations, especially while under imposed sliding, addressing, also thanks to the careful active learning stages, known shortcomings of ML-based methods in describing very short-distance interactions [51]. The atomic configurations of the systems were collected every 10 femtoseconds along the trajectories obtained during the over 1 nanosecond simulation time span. Snapshots of the iron-gallate systems during sliding simulations were visualized using the OVITO visualization package [52].

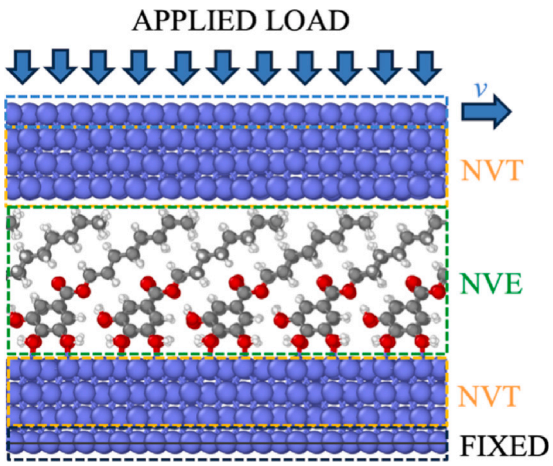

Fig. 1. Simulation model of a monolayer of gallate molecules confined between two Fe (110) substrates for MLIP simulations. Arrows represent the action of the applied pressure and of the constant sliding velocity constraint on the topmost iron layer, identified by the dashed cyan perimeter. The dashed orange perimeters identify the two regions in which iron atoms are thermostatted (NVT label), while the green one the atoms subjected only to MLIP forces (NVE label). Finally the bottom-most dashed black perimeter identifies the reference iron layer, with fixed atomic positions.

3. Results

3.1. Adsorption of gallates on iron surface by ab initio calculations

The adsorption of gallate molecules onto the Fe(110) is driven by two competing mechanisms [35]. The high affinity between carbon and iron atoms favors the atomic configuration with the aromatic ring of the molecule laying down, parallel to the surface, with the formation of strong carbon-iron bridges (Fig. 2a–d), with an optimized geometry in which the molecule is somewhat distorted but remains intact. When the structural relaxation is started with the ring perpendicular to the surface, other less stable, minima are obtained with the molecule intact and undistorted and linked to the surface by the formation of weaker bonds between two molecular oxygen and two iron atoms (Fig. 2e–h). However, for this perpendicular adsorption the energy gains are much smaller than the previous parallel adsorption case, i.e., $E_{ads} = -0.81, -0.82, -0.82, -0.89$ eV instead of $E_{ads} = -3.34, -3.90, -4.00, -4.59$ eV for PG, BG, OG, and LG, respectively.

Much more stable parallel adsorptions are obtained when one also considers the possibility for the molecules to chemisorb by breaking the OH bonds and removing the two hydrogen atoms from the two oxygen atoms close to the surface. In this case, shorter and much stronger Fe–O bonds are formed, and the adsorption energies become more comparable with the case of the parallel adsorption, $E_{ads} = -3.43, -3.45, -3.44, -3.52$ eV (Fig. 2i–l). Indeed, the establishment of Fe–O–C bridges on the iron surface after the removal of two hydrogen atoms, is in good agreement with the XPS spectra measured experimentally [53]. This suggests that the picture can be constructed from the single molecule adsorption energies may not be so complete and that other factors could play a role in favor of the perpendicular

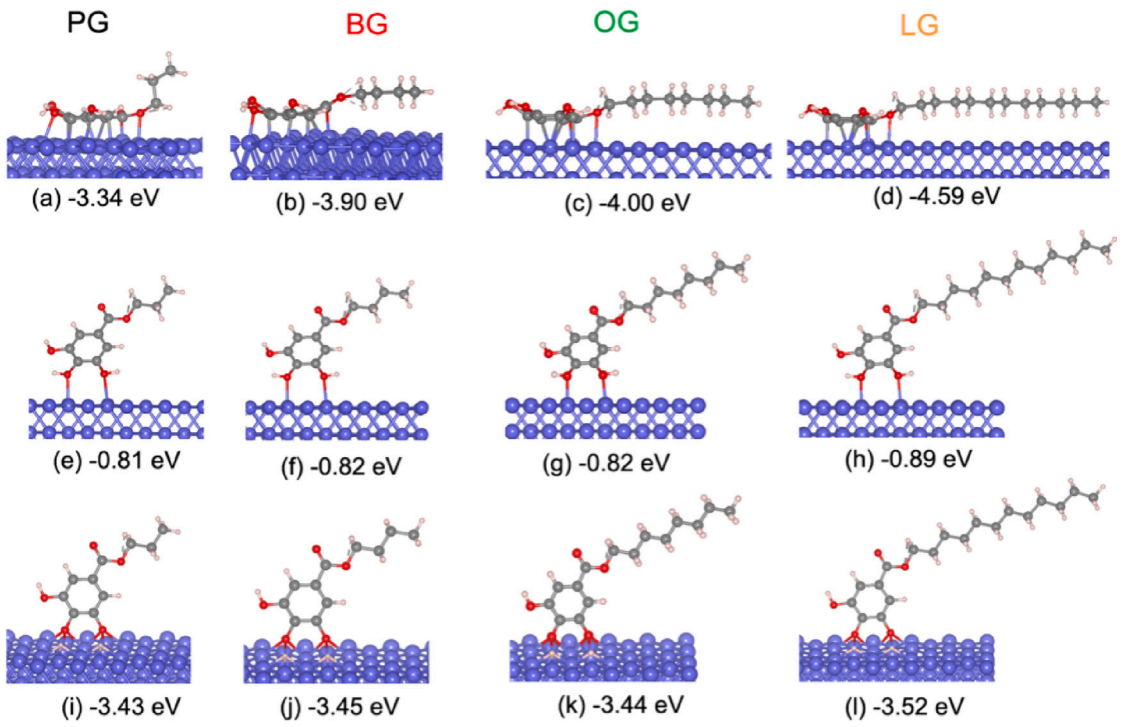

Fig. 2. Parallel (a–d), perpendicular (e–h), and dissociative (i–l) adsorption of one gallate molecule on Fe(110) surface.

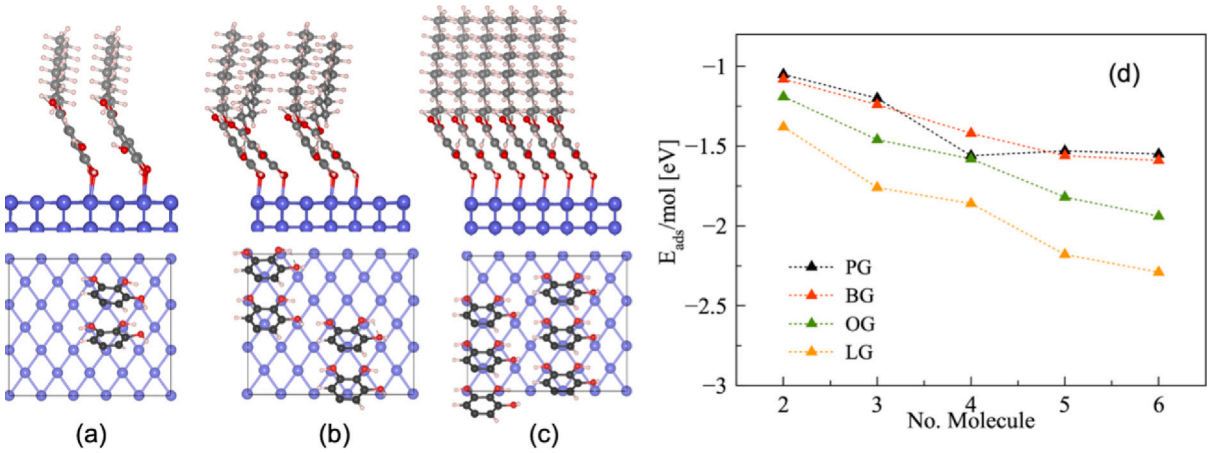

Fig. 3. Perpendicular adsorption of gallate molecules on Fe(110) surface: (a–c) top and side views of 2/4/6 molecules in a supercell. The hydrocarbon chains have been removed from the top views for clarity, each aromatic ring represents a gallate molecule. LG was selected as a representative, (d) adsorption energies as a function of coverage density.

adsorption geometry. In particular, since the molecules in the parallel adsorption configuration cover a much larger portion of the surface, one can expect the perpendicular adsorption to gain importance at high coverages with the molecules orderly packed to form a compact self-assembled monolayer with the alkyl chains all lined up parallel to each other [24,54].

To investigate the cooperative behavior of the gallate molecules the adsorption energies have been calculated as a function of the number of molecules perpendicularly adsorbed in the supercell, as shown in Fig. 3a–c. The study was performed with intact molecules to give them more freedom in the lateral displacements during the relaxation procedure. In the relaxed configurations, the molecules adsorb undistorted maintaining an ordered disposition which maximizes favorable vdW interactions between the alkyl chains and also the formation of hydrogen bonds across the molecules. A close packed monolayer structure is achieved when the Fe (110) surface of the supercell is covered with 6 molecules. The positions of the basal oxygen atoms are well in registry with the periodicity of the underlying lattice (Fig. 3c), resulting in the full coverage of the surface by a monolayer of gallate molecules. The adsorption energy per molecule shows a clear decreasing trend when the number of molecules per supercell increases, (Fig. 3d) making the perpendicular adsorption more stable with energy gains of ~0.5 eV for the shorter chains up to ~1 eV for the longer ones. Considering that the same gain makes the dissociated perpendicular chemisorption the lowest in energy for all the gallate molecules taken into account. Thus we can conclude that DFT predicts the formation of stable (self-assembled) monolayer (SAM) on the Fe (110) surface at full coverage, with the gallate molecules strongly anchored to the surface by the establishment of two strong Fe–O bonds per molecules.

3.2. Validation of the deep neural network potential

The energy and forces of the configurations put apart in the validation set and not included in the training datasets, have been compared

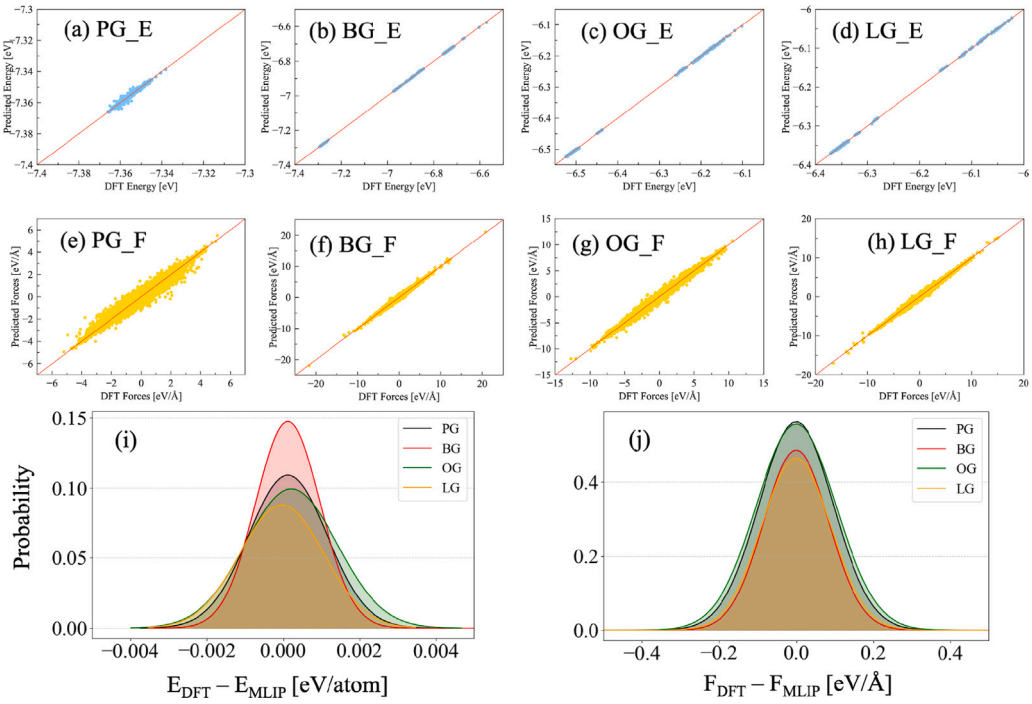

Fig. 4. Energies (a–d) and forces (e–h) calculated from the validation data by MLIP-MD simulations and DFT calculation for the confined models of gallate systems. Histogram distribution of the errors between MLIP prediction and DFT calculations for the energy (i) and for the forces (j).

with the energy and forces calculated by DFT. Results for each molecular system show a good agreement with the DFT values for both the energies, Fig. 4a–d, and the forces, Fig. 4e–h. For the energies, Fig. 4i, the RMSEs distribute mostly in the range from −0.002 to 0.002 eV/atom, with average values of 1.03×10^{-3}, 0.85×10^{-3}, 1.22×10^{-3}, and 1.09×10^{-3} eV/atom, for PG, BG, OG and LG, respectively. The RMSEs of forces, Fig. 4j, are 9.61×10^{-2}, 8.42×10^{-2}, 10.32×10^{-2} and 8.96×10^{-2} eV/A for PG, BG, OG and LG, respectively. Such values for the RMSEs are representatives of the typical accuracies that can be reached for complex systems of surfaces and interfaces, as reported in the literature, [30,31,35] and characterize a MLIP which is well capable of reproducing the accuracy of DFT calculations, albeit at a much lower computational cost.

3.3. Tribological properties from MLIP molecular dynamics simulations

MLIP molecular dynamics simulations were performed for systems with one SAM of gallate molecules confined between two iron slabs as depicted in Fig. 1. For each of the four molecular types (Fe-PG, Fe-BG, Fe-OG, and Fe-LG), initial configurations were generated with three number of molecules per unit area, $\rho = 0.0468, 0.0351, 0.0234$ Å^{-2} in the system, corresponding to a coverage of 100%, 66%, and 50% respectively. The full coverage systems were generated starting from the atomic configurations with 6 gallate molecules in a supercell obtained from the DFT structural optimizations. A MD supercell with a size of 42.6×36.14 Å^2 containing 72 gallate molecules in the SAM was constructed by a threefold replica of the DFT systems, with a total number of 4824, 5040, 5904, and 6768 atoms for PG, BG, OG, and LG, respectively. In all the systems there are always 1440×2 iron atoms forming the two identical slabs. The initial configurations for the intermediate 66.7% coverage was obtained by removing one third of the molecules from the DFT atomic configurations and then performing the same replica procedure, while the low 50% coverage was obtained by removing every other molecule from the full coverage models. The dynamics of each system was first integrated for a total period of 100 ps with only the applied load and at a temperature $T = 300$ K, in order to equilibrate the SAM confined between the two iron surfaces. At the end of the equilibration, the constraints imposing the sliding velocity $v = 50$ m/s were switched on, and the system dynamics integrated for a further 1 ns timespan.

For each system time averages were taken, on the final half nanosecond of the dynamical trajectories under load and sliding, for the frictional properties, i.e. the interfacial distance and the resistive force. The Fe-Fe separation $\Delta z = z_u - z_d$ is defined as the difference between the average vertical coordinate z_u of the iron atoms in the bottom-most layer of the upper slab and the average vertical coordinate z_d of the iron atoms in the uppermost layer of the lower slab. The resistive force F_x is calculated as the average force per unit area exerted by the constraints on the iron atoms moving at the constant relative sliding velocity v in the x direction.

The frictional properties of the Fe-gallate systems with different chain lengths at different coverages are presented in Fig. 5 by plotting the resistive force per unit area as a function of the Fe–Fe separation. More details are given in (Figure S2) and (Table S1).

At the full coverage, the Fe-Fe separations are maintained at large distances in all gallate systems. As the applied load increases, the separation between the two iron substrates decreases with a more significant reduction found in correspondence with the longer chains of OG and LG. It is worth mentioning that the roughly estimated lengths of the molecules as depicted in Figure S3 correlate well with the Fe-Fe separations, which remain stable during all the sliding (Figure S4), indicating the stability under the tribological conditions of the SAM layers, as in the initial DFT relaxed vertical configuration.

A similar distance-applied load relationship was found for the lower coverage systems. However, significant reductions in the Fe-Fe separations compared to those of the 100% coverage were recorded, with values much smaller than the length of the molecules and with a less pronounced dependence of the Fe–Fe separation on the chain length when the coverage density decreases. Overall, these results indicate that, at these lower coverages, there appear to be conformational changes relative to the initial SAM configuration, which can have a substantial impact on the frictional performance.

At low applied loads (0.5 and 1.0 GPa), remarkably low friction was obtained for all gallate molecules at full coverage. Such close similarity

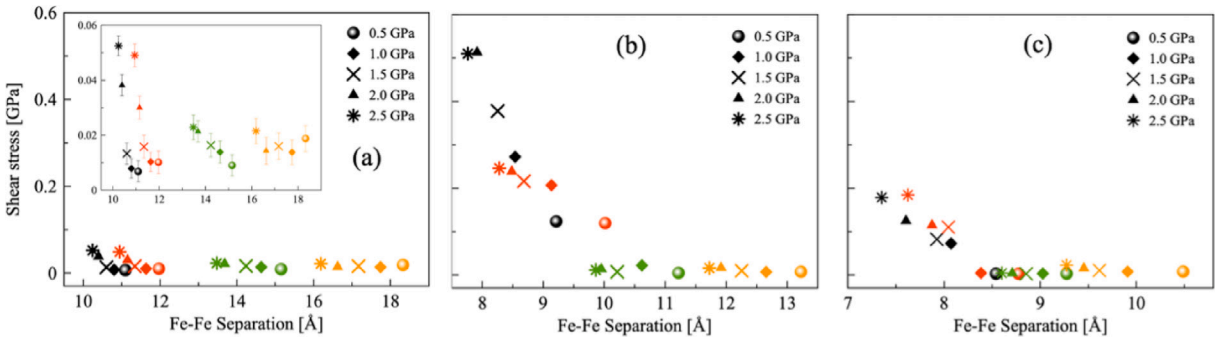

Fig. 5. Shear stress as a function of Fe–Fe separation in four gallate systems at different coverage densities: (a) 100%, (b) 66%, and (c) 50%. The insert in (a) details the shear stress behavior at a smaller scale. Color assignment: PG (Black), BG (Red), OG (Green), and LG (Orange).

can be explained by a friction mechanism which is mostly controlled by the Pauli repulsion between the upper iron substrate and the flat surface formed by close-packed hydrocarbon tails of the gallates molecules, regardless of the chain length [24,27]. As the applied load increases, the friction force maintains a low value only for the two molecules with the longest chains, OG and LG, while it goes up sharply starting from 1.5 GPa load for the molecules with the shorter chains, PG and BG.

At the lower coverages, friction remains consistently low for both the systems with OG and LG molecules. This result confirms that the molecules with the longer chains are very effective in reducing friction in all conditions, even at low densities, but, on the other hand, they indicate that another different mechanism concurs in providing the ultra-low friction. The chain length effect is more pronounced when the lubricant additives form a loosely packed monolayer. Indeed, at low coverages extremely high friction was recorded for the systems with PG and BG molecules, especially at 66% coverage, where the resistive forces of PG and BG systems are much greater than for OG and LG, regardless of the applied load value.

In order to understand the underlying microscopic mechanism a closer study of the structure of the monolayer is needed to understand what leads to the ultra-low friction of the long chain tribofilms and the high friction of the short chain tribofilms at the different coverage densities that is clearly exposed in Fig. 5a–c.

3.4. Friction reduction mechanisms

The snapshots of the Fe-gallate systems at full coverage are presented in Fig. 6a–d at the sliding time of 500 ps and 2 GPa, together with the densities of each atomic species along the vertical direction (Fig. 6e–h). For all systems, the SAM configuration is well conserved during the sliding, and it is stabilized by the Fe–O–C bridges as a result of the H detachment from the Fe–OH bonds. It is well-known that iron surface is highly catalytic [55] which can facilitate the spontaneous dissociation of the OH bonds near the surface [56]. In Figure S5 the dynamical behavior of the number of Fe–H/Fe–O/Fe–C bonds present during the simulations is shown as a function of time. H, O and C atoms are considered bonded to Fe if their distance from the iron surface is less than 1.8, 2.3 and 2.3 Å, respectively. In all cases, the OH dissociation at Fe–OH bonds occurs immediately starting from the thermalization process under load, indicating, consistently with the DFT calculations, a more stable dissociative form than the molecular adsorption. The formation of Fe–O bonds is also associated with the adsorption of the detached hydrogen atoms onto the lower surface. Under high (2 GPa) loads, diffusion of hydrogen atoms into the iron lower substrate can be observed, as it is indicated by the presence of the tail of the hydrogen density curves in the iron region (Fig. 6e–h). It is worth mentioning that the OH bond dissociation results in multiple Fe–O–C bonds that play a crucial role to maintain the adhesion between the SAM and the surface, thus keeping the SAM attached to the surface under shearing conditions [54]. Indeed no decrease of the large number of Fe–O bonds is observed during sliding at the lower iron surface. On the other hand, some presence of Fe–C bonds at the lower iron surface can be seen in Figure S5 due to the tilting under load of few gallate molecules, that brings their aromatic rings closer to the surface. However, the tightly packed configurations at high coverage promote hydrogen bonding and vdW interactions across the molecules. These interchain interactions keep the gallate molecules stand vertically and stabilize the SAM structures under harsh conditions. The hydrocarbon tails remain intact in the studied range of loads.

In all systems, apart from rare exceptions, all molecules stand vertically with the last three/four –CH_x groups of the alkyl chains flattened by the concerted action of compression and sliding. This behavior is featured by a sharp peak in the density profiles near the upper iron substrate. In both the short-chain and the long-chain systems, these flat layers are well-ordered (Figure S6) and evenly distributed, and can be assumed to be responsible for load bearing and friction reduction. Bond formation at the upper iron surface is almost absent, but for the short-chain systems of PG and BG (Figure S5a, b) where some short-lived Fe–O and Fe–C bonds can be formed. The flattening of the hydrocarbon tails, however, also makes the distance between the highest oxygen atom of the molecules and the upper surface shorter, particularly in the short-chain systems PG and BG when the load increases. With the short chain, the hydrocarbon tails are unable to maintain the oxygen far from the iron atoms to avoid their strong interaction. The higher the load the closer are Fe and O atoms. As a result, also oxygen atoms are present in the flat hydrocarbon regions and chemical bonds can be formed between this oxygen of the molecule and an interfacial iron atom (Fe_u) of the upper substrate. The possibility of formation of Fe_u–O bonds is indicated by a small peak in the oxygen density profile at ~14 Å, with a reduced Fe_u–O distance of ~2.1 to 2.3 Å (Fig. 6e). Thus, the high friction found in the short-chain systems can be primarily associated with the intermittent formation of the Fe_u–O bonds across the interface. This behavior, on the contrary, is not present for the OG and LG systems thanks to large Fe_u–O distances guaranteed by the presence of the long alkyl chains. Thus, the low friction of the Fe-gallate systems at high coverage can be directly associated with the role played the alkyl chains in the stable, well-ordered, SAM.

For the lower coverages, snapshots of the PG and OG configurations at 2 GPa and the corresponding density profiles are shown in Fig. 7 as representatives of the short- and long-chain systems. It is evident that the reduction of the Fe–Fe separation shown in Fig. 5b–c is associated with the loss of the vertical orientation of the gallate molecules at low coverages (Fig. 7a–d) [57]. The aromatic rings fall parallel to and adsorb on the Fe surface, filling the empty space left by the removal of gallate molecules from the corresponding 100%-coverage system. The formation of Fe–C bonds at the lower iron surfaces dominates the bond formation in all systems, as it is clearly seen in Figure S7. Multiple Fe–C chemical bonds are formed between carbon atoms of the aromatic rings and the surface, similarly to the parallel adsorption configurations obtained from the DFT optimization and shown in Fig. 2a–d, leading

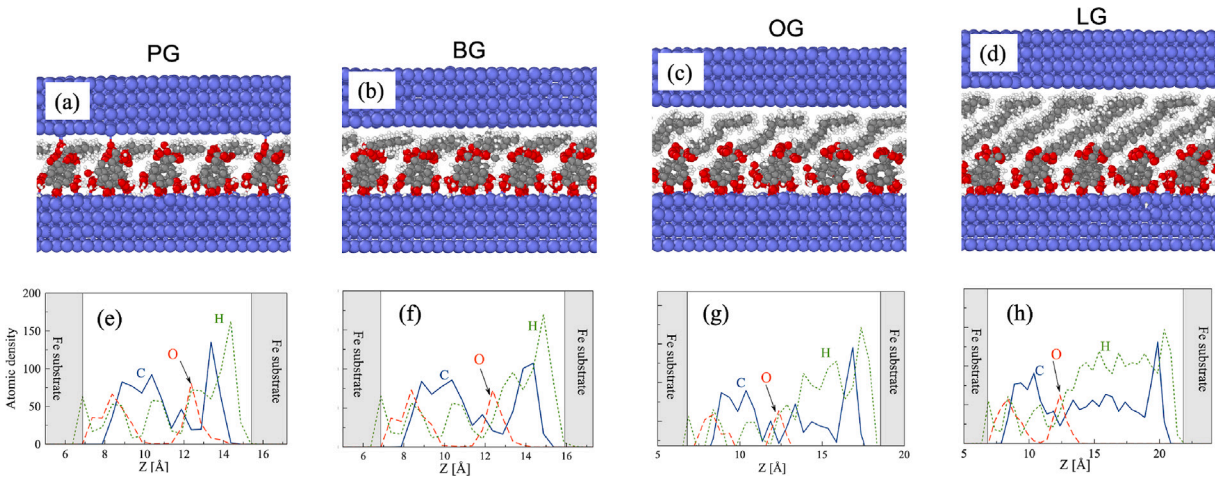

Fig. 6. Snapshots of Fe–gallate systems at full coverage (a–d) and their corresponding atomic density vertical profiles averaged over a 10 ps timespan centered around time t = 500 ps during the sliding process under a 2 GPa load (e–h).

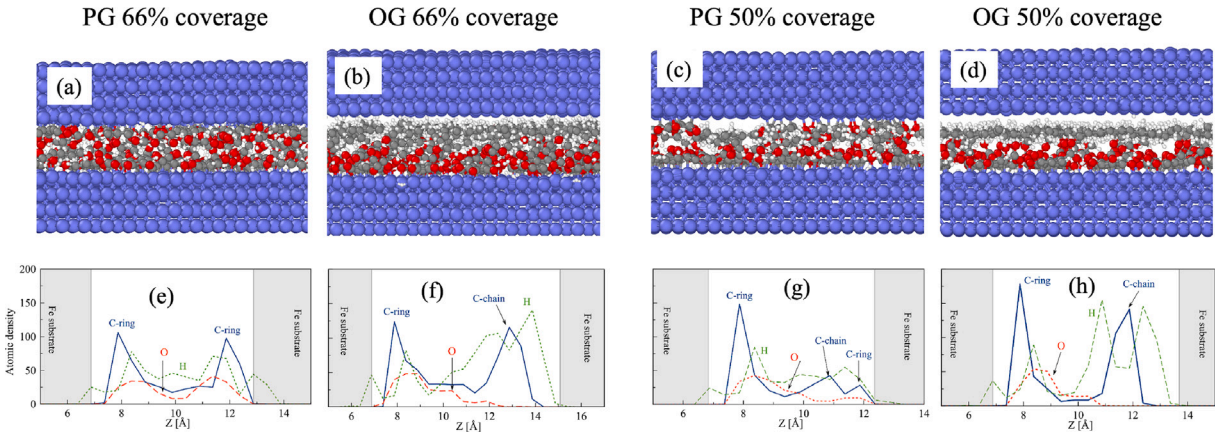

Fig. 7. Snapshots of PG and OG, representing short- and long-chain sliding systems (a–d), respectively, are presented alongside their corresponding density profiles averaged over a 10 ps timespan centered around time$t$ = 500 ps during the sliding process under a 2 GPa load (e–h).

to significant number of Fe–C bonds compared to that of Fe–O or Fe–H bonds. In addition, larger distances are present between the molecular chains and this ultimately results in the loss of hydrogen bonding and reduced vdW attraction across molecules and, eventually, in the collapse of the gallate SAM. The ordered SAM collapse creates a tribofilm characterized by an adsorbed layer of the aromatic rings and by the formation of Fe–C and Fe–O bonds at the interface, as it is indicated by the first sharp peaks in the carbon and oxygen density profiles near the iron lower substrate. The number of Fe–O and Fe–H bonds at the lower surface quickly increases during thermalization under load (Figure S7) to reach an equivalent value per molecule similarly to the full coverage systems, meaning that O–H bond dissociation occurs at the Fe–OH bonds. The higher number of carbon atoms and the sharper peaks near the lower iron surface in the profiles of the half-coverage systems (Fig. 7g–h) compared to those of the 66% coverage demonstrate a complete transformation of the aromatic ring orientations from the perpendicular to the parallel adsorption in the 50% coverage systems. The adsorption layer fully covers the iron surface and thus can still play the role of a protective layer to prevent surface damage.

The flattening of the aromatic rings onto the surface is not so effective, leaving vacant spaces, in the short-chain systems. Thus, a small fraction of PG molecules can move towards the upper iron surface, as shown in Figs. 7a and 7c. These molecules are adsorbed on the upper surface by the bonding between iron atoms and C and O of aromatic rings, as it is indicated by a small peak near the upper surface in the density profiles of carbon and oxygen (Figs. 7e and 7g). Bond formation at the upper surface can be found in PG systems for Fe–C, Fe–O, and Fe–H bonds, as shown in Figures S7a-b. Overall, this leads to the creation of tribofilms with a disordered structure and the molecular layer at the sliding interface presenting a mix of hydrocarbon tails and aromatic rings. As a results, a significant increase in friction was found for the short-chain systems at low coverages. In contrast, in the longer-chain systems, a conformational transformation occurs not only for the aromatic ring orientations but also for the orientation of the hydrocarbon tails. Particularly, under sliding condition, the alkyl chains reorganize to form a packed hydrocarbon layer parallel to the upper surface. Unlike the short-chain system PG, no chemical bonds form at the upper iron surface (Figures S7c–d). Thus, in the long chain systems, there are two well distinguished carbon layers along the z direction, one for the aromatic ring and another for the hydrocarbon tails. These features are highlighted by the two distinct sharp peaks in the carbon density profiles in Fig. 7f, h, more pronounced in the half-coverage system (Fig. 7f). This is due to the fact that in the 50%-coverage system, on the iron surface the vacant space is larger and, with a distribution of molecules more even and uniform, all the molecules have enough space to undergo the upright-to-flat geometrical transformation (Figure S8). In the 66% coverage system, the density profiles show that there are carbon atoms present in the region between the peaks corresponding to the ring and to the tail layers, implying that a portion of the molecules remains upright. On the other hand, thanks to the larger sizes, the longer alkyl chains can still fill up the vacant space left by the flattening of the carbon rings, and prevent the migration of OG molecules towards

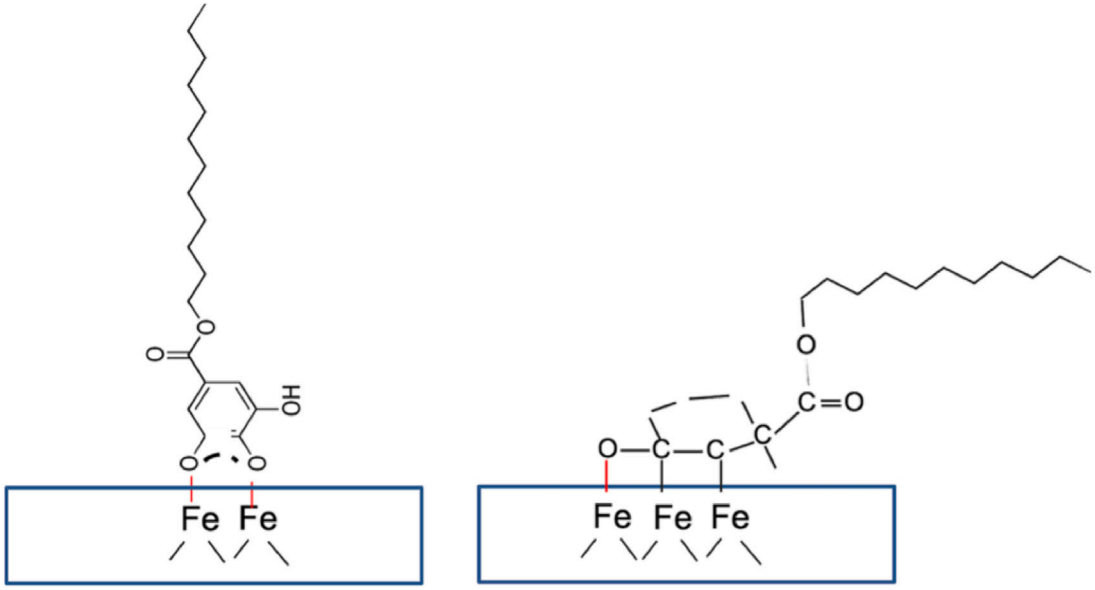

Fig. 8. Two proposed mechanisms of friction reduction by gallate molecules: (a) the formation of a SAM and (b) the formation of double carbon layer.

the upper surface. More importantly, the parallel orientation of the hydrocarbon tails creates a supportive layer for friction and loads, where Pauli repulsion dominates resulting in extremely low friction for these long-chain systems. This means that a uniform distribution of the molecules plus sufficiently long chains to effectively fill space can still be highly beneficial for friction even at lower concentrations, and that the friction reduction mechanism here described can be used to tune the frictional performance by modifying the coverage density as well as the chain length of the lubricant additive.

4. Discussion

The frictional results summarized in Fig. 5 show that either at high or low coverages, the longer alkyl chains of the OG and LG molecules outperform the friction reduction property of the shorter PG and BG counterparts, a result which is in good agreement with the experiment showing that lower friction is obtained with longer chains of gallate [53]. The behavior becomes more clear at lower coverage densities. From the analyses of the molecular structures of the gallate system under sliding conditions, we propose a twofold mechanisms of friction reduction associated with low- and high- coverage systems as depicted in Fig. 7. At the full coverage, the friction reduction behavior can be explained by the fact that the molecular layers are tightly packed. The breaking of OH bonds to form direct Fe–O–C bridges together with the interchain interactions stabilize the SAM and molecules remain upright throughout the sliding process (Fig. 6). As a result, the low friction is controlled by the direct contact of the tails of the tightly-packed hydrocarbon chains and the iron surface in all systems [57]. This explains the magnitudes of the resistive forces are relatively consistent with only a minor increase in the case of the shorter chain lengths.

The frictional performance depends even in a more pronounced way on the chain length when the tribofilms are loosely packed. While OG and LG maintain low friction, PG and BG have extremely high friction, particularly as the applied load increases. In addition, the significant reduction in the Fe–Fe separation compared to the full-coverage systems suggests that different mechanisms drives the high friction of the short chains and the ultra-low friction of the long chains. A first mechanism is based on the formation of a well-ordered SAM layer in which the head groups are stabilized by the formation of Fe–O–C chemical bonds as a result of OH bond dissociation and the tail groups are the hydrocarbon chains playing the key role of friction supportive layer (Fig. 8a). A second mechanism is related to the formation of two distinct carbon layers in which one layer is composed of aromatic rings, covering the surface and another layer is formed by the alkyl chains oriented parallel to the surface (Fig. 8b). This creates a flat layer of hydrocarbon chains near the upper iron surface, over which the load is distributed more evenly and the Pauli repulsions and weak vdW interactions dominate. Both mechanisms are promoted by the tribochemical reactions between the iron surface and the head groups of the gallate molecules that permit the formation of these stable carbon layers and reduce friction thanks to the cushion region filled with well-ordered hydrocarbon chains.

The effective elimination of chemical interactions between gallate molecules and the counter iron surface, with the formation of a stable well-ordered hydrocarbon layer, are the factors that play the friction reducing role and are secured by the sufficiently long chain, i.e. those of the OG and LG molecules that have been proven to provide better frictional performances compared to BG and PG.

These simulations highlights the need of using a reliable potential that can accurately describe friction-induced chemical reactions and the importance of statistical large scale models with simulation long enough to permit the systems to reach stationary condition, with a timescale of several hundred picoseconds in the systems we studied that it is not possible to explore with sufficient accuracy by ab initio molecular dynamics. The present molecular dynamics simulations based on machine learning interaction potentials achieve this goal with results that not only show a good agreement with the experiment but also permit to better understand the underlying atomistic mechanisms and, thus, to give an interpretation of the frictional properties.

A parallel investigation was carried out taking the ReaxFF from Shin et al. [46]. We report here as an example the results from the simulation of the OG gallate systems at 1 GPa, performed with an identical setup to that of the MLIP-MD simulations. A comparison of the structural properties of the systems obtained with the ReaxFF and the MLIP force fields is presented in Fig. 9. The analysis of the radial distribution function (RDF) at 1 GPa shows that the DNN potential predicts with DFT accuracy the chemical interactions at the interface, with Fe–O and Fe–C peaks around 1.8–2.2 Å, while ReaxFF fails to describe chemical bonds that characterize the adsorption of gallates on the iron- surface, which is one the critical factor that define the stability of the SAM in the systems. The ReaxFF force field overestimates the Fe–O bond distances, with an Fe–O peak at 3 Å in the 100% coverage system (Fig. 9a,d), while it underestimates the Fe–O bonds (~1.5 Å) in

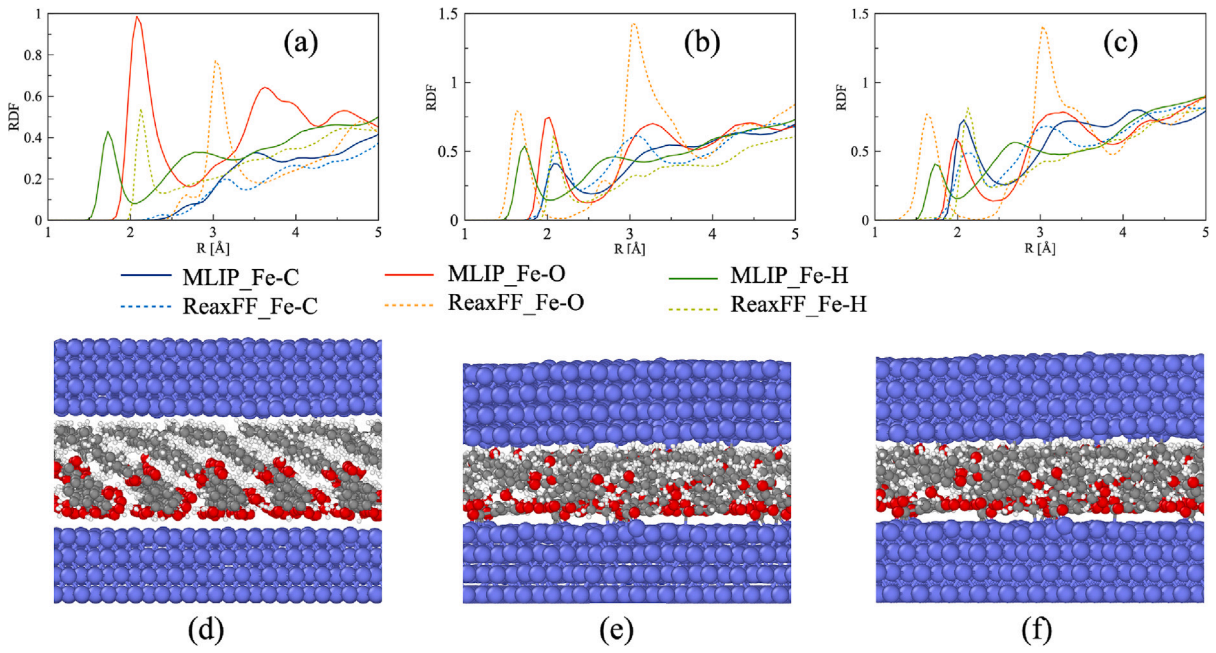

Fig. 9. Radial distribution functions obtained from the MLIP and MD simulations using ReaxFF for Fe-OG systems at 1 GPa and 1 ns at (a) full, (b) 66% and (c) 50% coverage. Snapshots of the Fe-OG systems at 1 GPa and 500 ps by ReaxFF MD simulations at (d) full, (e) 66% and (f) 50% coverage.

the 66% and 50% coverage systems (Fig. 9b, c). Chemical interactions can be found in the 66% and 50% coverage systems, but the bond formation is mostly based on the non-bridging oxygen and one or two carbon atoms of the aromatic rings with the iron atoms of the lower surface (Fig. 9e, f), which is unlike what can be obtained with the DFT optimizations, as shown in Fig. 2a–d. The mechanisms suggested by the reaxFF simulations lead to the displacement of some OG molecules from the lower surface to the upper one, and are able to create only a disordered lubricant layer, which is not as lubricious as the SAM, with frictional property massively affected. Therefore, results from simulations with empirical and reactive force fields should be taken with due care. The interaction potential should be carefully trained and validated for the specific system in order to obtain reliable statistical results as well as to provide meaningful atomistic mechanisms and also to be extended to other systems. Training specific machine learning interaction potentials to describe the system under study do achieve the required accuracy.

5. Conclusion

In this work, we have trained a MLIP based on *ab initio* data for tribological systems consisting of iron slabs lubricated by eco-friendly gallate molecules. The MLIP reproduces *ab initio* accuracy and enabled us to simulate tribological conditions in the systems where chemical reactions occur. We have performed large scale MLIP MD simulations to investigate frictional properties and understand the atomistic mechanisms of friction reduction of the gallate lubricants. We found that gallate molecules can organize to form a SAM on the iron surface at high coverage density that behaves as a very effective lubricious tribofilm. Under tribological condition, MLIP MD simulation results show that longer gallate chains (OG and LG) are more effective than shorter chains (PG and BG) in providing lower friction and larger interfacial separation, in agreement with what is found experimentally. The different performance of the shorter and longer gallate chains is better distinguishable at lower coverage densities of 66 and 50%.

Notably, we identify two atomistic mechanisms associated with friction reduction at high and low coverage densities. In particular, at high coverage density, the hydrocarbon chains of the SAM formed from upright adsorbed configurations of gallate molecules is responsible for supporting the frictional activity in the systems. The SAM is stabilized by the Fe–O–C bridges as a result of OH bond dissociation on the iron surface. Hydrogen bonds across molecules also help to lower the energy and to maintain the order of the hydrocarbon tails. The high friction found in the shorter chain systems (PG and BG) is associated with the formation of Fe–O chemical bonds across the interface at high applied loads.

At low coverage density, more clearly visible in the half coverage case, a double carbon layer is formed in the systems by the adsorption of aromatic rings onto the lower surface and by the orientation of the hydrocarbon chains parallel to the upper surface. The latter well-ordered hydrocarbon layer plays a key role as a friction reduction agent in the low coverage systems by forming a cushion were Pauli repulsions and weak vdW attraction dominate the interactions at the sliding interface. Meanwhile, the extremely high friction experienced in the short chain systems is due to the disordered state in the gallate layer under tribological conditions. These findings provide in-depth understanding for the interpretation of the frictional performance of gallate lubricants observed by experiments, and uncover key, general mechanisms that can help in designing effective additives for green lubricants.

CRediT authorship contribution statement

Huong Thi Thuy Ta: Writing – review & editing, Writing – original draft, Visualization, Software, Methodology, Investigation, Data curation. **Mauro Ferrario:** Writing – review & editing, Writing – original draft, Visualization, Methodology, Investigation, Formal analysis, Data curation. **Sophie Loehlé:** Writing – review & editing, Investigation, Formal analysis, Conceptualization. **Maria Clelia Righi:** Writing – review & editing, Writing – original draft, Supervision, Methodology, Investigation, Funding acquisition, Formal analysis, Conceptualization.

Declaration of competing interest

The authors declare that they have no known competing financial interests or personal relationships that could have appeared to influence the work reported in this paper.

Acknowledgments

The authors are happy to acknowledge their gratitude to Jean Michel Martin and Marie-Isabel De Barros-Bouchet for raising the interest on gallates, their advices and stimulating discussions. These results are part of the "Advancing Solid Interface and Lubricants by First-Principles Material Design (SLIDE)" project that has received funding from the European Research Council (ERC) under the European Union's Horizon 2020 research and innovation program (Grant Agreement No. 865633). Furthermore, we acknowledge the CINECA award under the ISCRA initiative, for the availability of high performance computing resources and support.

Appendix A. Supplementary data

Supplementary material related to this article can be found online at https://doi.org/10.1016/j.apsusc.2025.162836.

Data availability

Data will be made available on request.

References

[1] P. Nowak, K. Kucharska, M. Kamiński, Ecological and health effects of lubricant oils emitted into the environment, Int. J. Environ. Res. Public Heal. 16 (16) (2019) http://dx.doi.org/10.3390/ijerph16163002, URL https://www.mdpi.com/1660-4601/16/16/3002.

[2] S. Boyde, Green lubricants, environmental benefits and impacts of lubrication, Green Chem. 4 (2002) 293–307, http://dx.doi.org/10.1039/B202272A, URL http://dx.doi.org/10.1039/B202272A.

[3] Y. Jiang, J. Pei, Y. Zheng, Y.-j. Miao, B.-z. Duan, L.-f. Huang, Gallic acid: A potential anti-cancer agent, Chin. J. Integr. Med. 28 (7) (2022) 661–671, http://dx.doi.org/10.1007/s11655-021-3345-2.

[4] J. Bai, Y. Zhang, C. Tang, Y. Hou, X. Ai, X. Chen, Y. Zhang, X. Wang, X. Meng, Gallic acid: Pharmacological activities and molecular mechanisms involved in inflammation-related diseases, Biomed. Pharmacother. 133 (2021) 110985, http://dx.doi.org/10.1016/j.biopha.2020.110985, URL https://www.sciencedirect.com/science/article/pii/S075333222031177X.

[5] A. Perez, D.A. Basketter, I.R. White, J. McFadden, Positive rates to propyl gallate on patch testing: a change in trend, Contact Dermatitis 58 (1) (2008) 47–48, http://dx.doi.org/10.1111/j.1600-0536.2007.01150.x.

[6] H. Hamishehkar, S. Khani, S. Kashanian, J. Ezzati Nazhad Dolatabadi, M. Eskandani, Geno- and cytotoxicity of propyl gallate food additive, Drug Chem. Toxicol. 37 (3) (2014) 241–246, http://dx.doi.org/10.3109/01480545.2013.838776.

[7] M. Leopoldini, T. Marino, N. Russo, M. Toscano, Antioxidant properties of phenolic compounds: H-atom versus electron transfer mechanism, J. Phys. Chem. A 108 (22) (2004) 4916–4922, http://dx.doi.org/10.1021/jp037247.

[8] B. Badhani, N. Sharma, R. Kakkar, Gallic acid: a versatile antioxidant with promising therapeutic and industrial applications, RSC Adv. 5 (35) (2015) 27540–27557, http://dx.doi.org/10.1039/C5RA01911G, URL http://dx.doi.org/10.1039/C5RA01911G.

[9] F.T. Hong, A. Schneider, S.M. Sarathy, Enhanced lubrication by core–shell tio2 nanoparticles modified with gallic acid ester, Tribol. Int. 146 (2020) 106263, http://dx.doi.org/10.1016/j.triboint.2020.106263, URL https://www.sciencedirect.com/science/article/pii/S0301679X20301055.

[10] M.A. Fazal, F. Sundus, H.H. Masjuki, S. Rubaiee, M.M. Quazi, Tribological assessment of additive doped b30 biodiesel-diesel blend by using high frequency reciprocating rig test, Sustain. Energy Technol. Assess. 48 (2021) 101577, http://dx.doi.org/10.1016/j.seta.2021.101577, URL https://www.sciencedirect.com/science/article/pii/S2213138821005919.

[11] W. Tang, B. Wang, G. Wen, Y. Li, The distinguished long-term friction reduction and anti-wear functions of amphipathic carbon dots originated from lauryl gallate, Mater. Today Commun. 29 (2021) 102881, http://dx.doi.org/10.1016/j.mtcomm.2021.102881, URL https://www.sciencedirect.com/science/article/pii/S2352492821008692.

[12] H.T.T. Ta, N.V. Tran, A.K. Tieu, H. Zhu, H. Yu, T.D. Ta, Computational tribochemistry: A review from classical and quantum mechanics studies, J. Phys. Chem. C 125 (31) (2021) 16875–16891, http://dx.doi.org/10.1021/acs.jpcc.1c03725.

[13] A.I. Vakis, V.A. Yastrebov, J. Scheibert, L. Nicola, D. Dini, C. Minfray, A. Almqvist, M. Paggi, S. Lee, G. Limbert, J.F. Molinari, G. Anciaux, R. Aghababaei, S. Echeverri Restrepo, A. Papangelo, A. Cammarata, P. Nicolini, C. Putignano, G. Carbone, S. Stupkiewicz, J. Lengiewicz, G. Costagliola, F. Bosia, R. Guarino, N.M. Pugno, M.H. Müser, M. Ciavarella, Modeling and simulation in tribology across scales: An overview, Tribol. Int. 125 (2018) 169–199, http://dx.doi.org/10.1016/j.triboint.2018.02.005, URL https://www.sciencedirect.com/science/article/pii/S0301679X18300756.

[14] S. Loehlé, M.C. Righi, Ab initio molecular dynamics simulation of tribochemical reactions involving phosphorus additives at sliding iron interfaces, Lubricants 6 (2) (2018) http://dx.doi.org/10.3390/lubricants6020031.

[15] H.T.T. Ta, A.K. Tieu, H. Zhu, H. Yu, N.V. Tran, B.H. Tran, S. Wan, T.D. Ta, Ab initio study on physical and chemical interactions at borates and iron oxide interface at high temperature, Chem. Phys. 529 (2020) 110548, http://dx.doi.org/10.1016/j.chemphys.2019.110548, URL https://www.sciencedirect.com/science/article/pii/S0301010419308195.

[16] N.V. Tran, A. Kiet Tieu, H. Zhu, H.T.T. Ta, P.T. Sang, H.M. Le, T.D. Ta, Insights into the tribochemistry of sliding iron oxide surfaces lubricated by sodium silicate glasses: An ab initio molecular dynamics study, Appl. Surf. Sci. 528 (2020) 147008, http://dx.doi.org/10.1016/j.apsusc.2020.147008, URL https://www.sciencedirect.com/science/article/pii/S0169433220317657.

[17] C.J. Carkner, N.J. Mosey, Slip mechanisms of hydroxylated α-al2o3 (0001)/(0001) interfaces: A first-principles molecular dynamics study, J. Phys. Chem. C 114 (41) (2010) 17709–17719, http://dx.doi.org/10.1021/jp1055478.

[18] C.J. Carkner, S.M. Haw, N.J. Mosey, Effect of adhesive interactions on static friction at the atomic scale, Phys. Rev. Lett. 105 (5) (2010) 056102, http://dx.doi.org/10.1103/PhysRevLett.105.056102, URL https://link.aps.org/doi/10.1103/PhysRevLett.105.056102.

[19] M.-I. De Barros Bouchet, G. Zilibotti, C. Matta, M.C. Righi, L. Vandenbulcke, B. Vacher, J.-M. Martin, Friction of diamond in the presence of water vapor and hydrogen gas, coupling gas-phase lubrication and first-principles studies, J. Phys. Chem. C 116 (12) (2012) 6966–6972, http://dx.doi.org/10.1021/jp211322s.

[20] H.T.T. Ta, N.V. Tran, M.C. Righi, Nanotribological properties of oxidized diamond/silica interfaces: Insights into the atomistic mechanisms of wear and friction by ab initio molecular dynamics simulations, ACS Appl. Nano Mater. 6 (18) (2023) 16674–16683, http://dx.doi.org/10.1021/acsanm.3c02881.

[21] M. Cutini, G. Forghieri, M. Ferrario, M.C. Righi, Adhesion, friction and tribochemical reactions at the diamond–silica interface, Carbon 203 (2023) 601–610, http://dx.doi.org/10.1016/j.carbon.2022.11.074, URL https://www.sciencedirect.com/science/article/pii/S0008622322009952.

[22] S. Loehlé, C. Matta, C. Minfray, T. Mogne, R. Iovine, Y. Obara, A. Miyamoto, J. Martin, Mixed lubrication of steel by c18 fatty acids revisited, part i: Toward the formation of carboxylate, Tribol. Int. 82 (2015) 218–227, http://dx.doi.org/10.1016/j.triboint.2014.10.020, URL https://www.sciencedirect.com/science/article/pii/S0301679X14003776.

[23] S. Loehlé, C. Matta, C. Minfray, T. Le Mogne, R. Iovine, Y. Obara, A. Miyamoto, J. Martin, Mixed lubrication of steel by c18 fatty acids revisited, part ii: Influence of some key parameters, Tribol. Int. 94 (2016) 207–216, http://dx.doi.org/10.1016/j.triboint.2015.08.036, URL https://www.sciencedirect.com/science/article/pii/S0301679X15003783.

[24] C.A. Latorre, J.P. Ewen, C. Gattinoni, D. Dini, Simulating surfactant–iron oxide interfaces: From density functional theory to molecular dynamics, J. Phys. Chem. B 123 (31) (2019) 6870–6881, http://dx.doi.org/10.1021/acs.jpcb.9b02925.

[25] B. Park, M. Chandross, M.J. Stevens, G.S. Grest, Chemical effects on the adhesion and friction between alkanethiol monolayers: Molecular dynamics simulations, Langmuir 19 (22) (2003) 9239–9245, http://dx.doi.org/10.1021/la0341106.

[26] K. Ahmad, Q. Yang, A. Martini, Simulations of friction anisotropy on self-assembled monolayers in water, Langmuir 38 (20) (2022) 6273–6280, http://dx.doi.org/10.1021/acs.langmuir.1c03234.

[27] J.P. Ewen, C. Gattinoni, N. Morgan, H.A. Spikes, D. Dini, Nonequilibrium molecular dynamics simulations of organic friction modifiers adsorbed on iron oxide surfaces, Langmuir 32 (18) (2016) 4450–4463, http://dx.doi.org/10.1021/acs.langmuir.6b00586.

[28] O. Alexiadis, V.A. Harmandaris, V.G. Mavrantzas, L.D. Site, Atomistic simulation of alkanethiol self-assembled monolayers on different metal surfaces via a quantum, first-principles parametrization of the sulfur–metal interaction, J. Phys. Chem. C 111 (17) (2007) 6380–6391, http://dx.doi.org/10.1021/jp067347u.

[29] M.F. Calegari Andrade, H.-Y. Ko, L. Zhang, R. Car, A. Selloni, Free energy of proton transfer at the water–tio2 interface from ab initio deep potential molecular dynamics, Chem. Sci. 11 (9) (2020) 2335–2341, http://dx.doi.org/10.1039/C9SC05116C, URL http://dx.doi.org/10.1039/C9SC05116C.

[30] Z. Li, X. Tan, Z. Fu, L. Liu, J.-Y. Yang, Thermal transport across copper–water interfaces according to deep potential molecular dynamics, Phys. Chem. Chem. Phys. 25 (9) (2023) 6746–6756, http://dx.doi.org/10.1039/D2CP05530A, URL http://dx.doi.org/10.1039/D2CP05530A.

[31] X.-T. Fan, X.-J. Wen, Y.-B. Zhuang, J. Cheng, Molecular insight into the gap(110)-water interface using machine learning accelerated molecular dynamics, J. Energy Chem. 82 (2023) 239–247, http://dx.doi.org/10.1016/j.jechem.2023.03.013, URL https://www.sciencedirect.com/science/article/pii/S2095495623001730.

[32] M. de la Puente, R. David, A. Gomez, D. Laage, Acids at the edge: Why nitric and formic acid dissociations at air–water interfaces depend on depth and on interface specific area, J. Am. Chem. Soc. 144 (23) (2022) 10524–10529, http://dx.doi.org/10.1021/jacs.2c03099.

[33] Y. Zhang, H. Huang, J. Tian, C. Li, Y. Jiang, Z. Fan, L. Pan, Modelling electrified microporous carbon/electrolyte electrochemical interface and unraveling charge storage mechanism by machine learning accelerated molecular dynamics, Energy Storage Mater. 63 (2023) 103069, http://dx.doi.org/10.1016/j.ensm.2023.103069, URL https://www.sciencedirect.com/science/article/pii/S2405829723004476.

[34] Y.-B. Zhuang, J. Cheng, Deciphering the anomalous acidic tendency of terminal water at rutile(110)–water interfaces, J. Phys. Chem. C 127 (22) (2023) 10532–10540, http://dx.doi.org/10.1021/acs.jpcc.3c01870.

[35] H.T.T. Ta, M. Ferrario, S. Loehlé, M.C. Righi, Ab initio informed machine learning potential for tribochemistry and mechanochemistry: Application for eco–friendly gallate lubricant additive, Comput. Mater. Today 1 (2024) 100005, http://dx.doi.org/10.1016/j.commt.2024.100005, URL https://www.sciencedirect.com/science/article/pii/S295046352400005X.

[36] P. Ying, A. Natan, O. Hod, M. Urbakh, Effect of interlayer bonding on superlubric sliding of graphene contacts: A machine-learning potential study, ACS Nano 18 (14) (2024) 10133–10141, http://dx.doi.org/10.1021/acsnano.3c13099.

[37] A. Pacini, M. Ferrario, S. Loehle, M.C. Righi, Advancing tribological simulations of carbon-based lubricants with active learning and machine learning molecular dynamics, Eur. Phys. J. Plus 139 (6) (2024) 549, http://dx.doi.org/10.1140/epjp/s13360-024-05348-z.

[38] G. Kresse, J. Furthmüller, Efficient iterative schemes for ab initio total-energy calculations using a plane-wave basis set, Phys. Rev. B 54 (16) (1996) 11169–11186, http://dx.doi.org/10.1103/PhysRevB.54.11169, URL https://link.aps.org/doi/10.1103/PhysRevB.54.11169.

[39] J.P. Perdew, K. Burke, M. Ernzerhof, Generalized gradient approximation made simple, Phys. Rev. Lett. 77 (18) (1996) 3865–3868, http://dx.doi.org/10.1103/PhysRevLett.77.3865, URL https://link.aps.org/doi/10.1103/PhysRevLett.77.3865.

[40] S. Grimme, Semiempirical gga-type density functional constructed with a long-range dispersion correction, J. Comput. Chem. 27 (15) (2006) 1787–1799, http://dx.doi.org/10.1002/jcc.20495.

[41] T. Bučko, J. Hafner, S. Lebègue, J.G. Ángyán, Improved description of the structure of molecular and layered crystals: Ab initio dft calculations with van der waals corrections, J. Phys. Chem. A 114 (43) (2010) 11814–11824, http://dx.doi.org/10.1021/jp106469x.

[42] H.N.S.M. Renguo Lu, Ichiro Minami, Investigation of decomposition of hydrocarbon oil on the nascent surface of steel, Tribol. Lett. 27 (2007) 25–30, http://dx.doi.org/10.1007/s11249-007-9203-3.

[43] K. Enami, H. Yamada, H. Komata, Hydrogen generation from lubricant under rolling-sliding contact, Tribol. Online 19 (4) (2024) 298–307, http://dx.doi.org/10.2474/trol.19.298.

[44] C.F. Tecle S. Rufael, James D. Batteas, The influence of surface oxidation on the reactions of methanol on fe(110), Surf. Sci. 384 (1997) 156–167, http://dx.doi.org/10.1016/S0039-6028(97)00197-0.

[45] A.P. Thompson, H.M. Aktulga, R. Berger, D.S. Bolintineanu, W.M. Brown, P.S. Crozier, P.J. in 't Veld, A. Kohlmeyer, S.G. Moore, T.D. Nguyen, R. Shan, M.J. Stevens, J. Tranchida, C. Trott, S.J. Plimpton, Lammps - a flexible simulation tool for particle-based materials modeling at the atomic, meso, and continuum scales, Comput. Phys. Comm. 271 (2022) 108171, http://dx.doi.org/10.1016/j.cpc.2021.108171, URL https://www.sciencedirect.com/science/article/pii/S0010465521002836.

[46] Y.K. Shin, H. Kwak, A.V. Vasenkov, D. Sengupta, A.C.T. van Duin, Development of a reaxff reactive force field for fe/cr/o/s and application to oxidation of butane over a pyrite-covered cr2o3 catalyst, ACS Catal. 5 (12) (2015) 7226–7236, http://dx.doi.org/10.1021/acscatal.5b01766.

[47] H. Wang, L. Zhang, J. Han, W. E, Deepmd-kit: A deep learning package for many-body potential energy representation and molecular dynamics, Comput. Phys. Comm. 228 (2018) 178–184, http://dx.doi.org/10.1016/j.cpc.2018.03.016, URL https://www.sciencedirect.com/science/article/pii/S0010465518300882.

[48] M. Abadi, P. Barham, J. Chen, Z. Chen, A. Davis, J. Dean, M. Devin, S. Ghemawat, G. Irving, M. Isard, M. Kudlur, J. Levenberg, R. Monga, S. Moore, D.G. Murray, B. Steiner, P. Tucker, V. Vasudevan, P. Warden, M. Wicke, Y. Yu, X. Zheng, Tensorflow: a system for large-scale machine learning, in: Proceedings of the 12th USENIX Conference on Operating Systems Design and Implementation, OSDI'16, USENIX Association, USA, 2016, pp. 265–283.

[49] L. Zhang, J. Han, H. Wang, W.A. Saidi, R. Car, E. Weinan, End-to-end symmetry preserving inter-atomic potential energy model for finite and extended systems, in: Proceedings of the 32nd International Conference on Neural Information Processing Systems, NIPS'18, Curran Associates Inc., Red Hook, NY, USA, 2018, pp. 4441–4451.

[50] Y. Zhang, H. Wang, W. Chen, J. Zeng, L. Zhang, H. Wang, W. E, Dp-gen: A concurrent learning platform for the generation of reliable deep learning based potential energy models, Comput. Phys. Comm. 253 (2020) 107206, http://dx.doi.org/10.1016/j.cpc.2020.107206, URL https://www.sciencedirect.com/science/article/pii/S001046552030045X.

[51] H. Wang, X. Guo, L. Zhang, H. Wang, J. Xue, Deep learning inter-atomic potential model for accurate irradiation damage simulations, Appl. Phys. Lett. 114 (24) (2019) 244101, http://dx.doi.org/10.1063/1.5098061.

[52] A. Stukowski, Visualization and analysis of atomistic simulation data with ovito–the open visualization tool, Modelling Simul. Mater. Sci. Eng. 18 (1) (2009) 015012, http://dx.doi.org/10.1088/0965-0393/18/1/015012.

[53] Y. Long, J.M. Martin, F. Dubreuil, B. Thiebaut, S. Loehlé, H.T.T.T. Ta, M. Ferrario, M.C. Righi, M.-I. De Barros Bouchet, Friction and wear reduction with alkyl gallate antioxidant food additives in pag–based aqueous lubricants, 2024.

[54] C. Gattinoni, J.P. Ewen, D. Dini, Adsorption of surfactants on α-fe2o3(0001): A density functional theory study, J. Phys. Chem. C 122 (36) (2018) 20817–20826, http://dx.doi.org/10.1021/acs.jpcc.8b05899.

[55] X. Yang, J. Dang, C. Zhang, J. Li, S. Niu, H. Gao, B. Liu, Z. Guo, H. Ma, Comparing the catalytic effect of metals for energetic materials: Machine learning prediction of adsorption energies on metals, Langmuir 40 (1) (2024) 1087–1095, http://dx.doi.org/10.1021/acs.langmuir.3c03348.

[56] M. Eder, K. Terakura, J. Hafner, Initial stages of oxidation of (100) and (110) surfaces of iron caused by water, Phys. Rev. B 64 (11) (2001) 115426, http://dx.doi.org/10.1103/PhysRevB.64.115426, URL https://link.aps.org/doi/10.1103/PhysRevB.64.115426.

[57] P.T. Mikulski, J.A. Harrison, Packing-density effects on the friction of n-alkane monolayers, J. Am. Chem. Soc. 123 (28) (2001) 6873–6881, http://dx.doi.org/10.1021/ja010189u.